ADVANCES IN ATMOSPHERIC SCIENCES, VOL. 29, NO. 3, 2012, 441–454

Predictability of the East Asian Winter Monsoon Interannual Variability as Indicated by the DEMETER CGCMS

LI Fei*[1,3] (李 菲) and WANG Huijun[1,2] (王会军)

[1] *Nansen-Zhu International Research Center, Institute of Atmospheric Physics, Chinese Academy of Sciences, Beijing* 100029

[2] *Climate Change Research Center, Chinese Academy of Sciences, Beijing* 100029

[3] *Graduate University of Chinese Academy of Sciences, Beijing* 100049

(Received 12 July 2011; revised 21 November 2011)

ABSTRACT

The interannual variability of East Asian winter monsoon (EAWM) circulation from the Development of a European Multi-Model Ensemble (MME) System for Seasonal to Inter-Annual Prediction (DEMETER) hindcasts was evaluated against observation reanalysis data. We evaluated the DEMETER coupled general circulation models (CGCMs)' retrospective prediction of the typical EAWM and its associated atmospheric circulation. Results show that the EAWM can be reasonably predicted with statistically significant accuracy, yet the major bias of the hindcast models is the underestimation of the related anomalies. The temporal correlation coefficient (TCC) of the MME-produced EAWM index, defined as the first EOF mode of 850-hPa air temperature within the EAWM domain (20°–60°N, 90°–150°E), was 0.595. This coefficient was higher than those of the corresponding individual models (range: 0.39–0.51) for the period 1969–2001; this result indicates the advantage of the super-ensemble approach. This study also showed that the ensemble models can reasonably reproduce the major modes and their interannual variabilities for sea level pressure, geopotential height, surface air temperature, and wind fields in Eurasia. Therefore, the prediction of EAWM interannual variability is feasible using multimodel ensemble systems and that they may also reveal the associated mechanisms of the EAWM interannual variability.

Key words: East Asian winter monsoon, interannual variability, DEMETER, hindcast

Citation: Li, F., and H. J. Wang, 2012: Predictability of the East Asian winter monsoon interannual variability as indicated by the DEMETER CGCMS. *Adv. Atmos. Sci.*, **29**(3), 441–454, doi: 10.1007/s00376-011-1115-3.

1. Introduction

The East Asian winter monsoon (EAWM) is one of the most active atmospheric circulation systems in boreal winter. Its southward bursts can affect the weather and climate over East Asia, Southeast Asia, South China Sea, and can even reach cross the equator and affect Australia (Zhang and Zhang, 2010). In this process, the EAWM can result in general cooling and sometimes in precipitation over the regions affected (e.g., snowfall in northern China and/or freezing rain in southern China), and therefore the EAWM can impact social and economical activities.

In the past, interest in EAWM research has been boosted by the increase in the frequency and severity of weather-related disasters in China that result from anomalous EAWMs. Particularly in January and early February 2008, an anomalously strong EAWM occurred with extremely low regional temperatures, blizzard conditions in northern China, and freezing rain in southern China (Zhou et al., 2009; Han et al., 2011). Previous studies have shown that the EAWM exhibits remarkable interannual and interdecadal variability (Ji et al., 1997; Zhang et al., 1997; Wang, 2001;

*Corresponding author: LI Fei, lifei-715@163.com

Chen et al., 2005; Zhu et al., 2005; Fan, 2009; Sun et al., 2010; Wang et al., 2009b, c, 2010, 2011). In addition, the EAWM year-to-year variations are recognized to respond to the ENSO (Webster and Yang, 1992; Zhang et al., 1996; Lau and Nath, 2000; Wang et al., 2000, 2008), Arctic Oscillation (AO; Gong et al., 2001; Wang and Sun, 2009), and Siberian high (Takaya and Nakamura, 2005a, b).

For much of the research on the EAWM, a reasonable definition of EAWM index is a prerequisite. Most researchers have used a simple circulation variable as an index to measure EAWM intensity, such as the east–west pressure contrast (e.g., Guo, 1994; Shi and Yang, 1998; Wang et al., 2009c), the 500-hPa East Asian trough (e.g., Cui and Sun, 1999; Wang et al., 2009b), the low-level wind (e.g., Wang and Jiang, 2004), or the upper-tropospheric zonal wind shear over East Asia (e.g., Jhun and Lee, 2004). Yan et al. (2009) developed an EAWM index that is a composite of surface air temperature, sea level pressure, and 500-hPa geopotential height. Wang and Chen (2010) presented a comprehensive review of EAWM indices. Here, we propose a new EAWM index based on low-level air temperature. This new index is somewhat based on phenomena, and it can capture the major features of EAWM circulation. This index can also be easily used for studies on the long-term variability of the EAWM because of the limited number of indicators or "proxies" of EAWM prior to the instrumental period.

In this study, we explored the predictability of EAWM interannual variability based on 33-year (1969–2001) retrospective predictions made by three of the DEMETER models, which provides a general understanding of the model's capability and the model improvement. The datasets and model experiments used are described in section 2. The definition of the EAWM index and model performance are documented in section 3 and section 4, respectively, while the discussion and summary follows in section 5.

2. Datasets and model description

The Development of a European Multimodel Ensemble (MME) System for Seasonal to Interannual Prediction Project (DEMETER) was conceived and funded under the European Union Fifth Framework Environment Programme (Palmer et al., 2004). Seven independent state-of-the-art models produced a series of 6-month ensemble hindcasts with common archiving systems and diagnostics. Each model was run nine times with different initial conditions, resulting in a global multimodel and multi–initial condition ensemble hindcasts.

In this study, we selected winter (December–February) hindcasts from three of seven DEMETER models [SCWF from European Centre for Medium-Range Weather Forecasts (ECMWF), CNRM from Météo-France, and SMPI from Max-Planck Institut für Meteorologie (MPI); see Table 1] because longer time series over a 33-year period from December 1969 to February 2002 were available for these models. To validate the model, we used the average of two monthly mean reanalysis datasets: NCEP-1 (Kalnay et al., 1996) and ERA-40 (Uppala et al., 2005). The fields

Table 1. Combinations of atmosphere and ocean models used by the three partners contributing with coupled models to DEMETER. The resolution of the models and the initialization strategy are outlined as well. The modeling partners are ECMWF (European Centre for Medium-Range Weather Forecasts, International Organization), Météo-France (Centre National de Recherches Météorologiques, Météo-France, France), and MPI (Max-Planck Institut für Meteorologie, Germany) (Palmer et al., 2004).

	ECMWF	Météo-France	MPI
Atmosphere component	IFS	ARPEGE	ECHAM-5
Resolution	T95 40 levels	T63 31 levels	T42 19 levels
Atmosphere initial conditions	ERA-40	ERA-40	Coupled run relaxed to observed SSTs
Reference	Gregory et al. (2000)	Déqué (2001)	Roeckner (1996)
Ocean component	HOPE-E	OPA 8.0	MPI-OM1
Resolution	$1.4° \times 0.3°$–$1.4°$ 29 levels	182 GP × 152 GP 31 levels	$2.5° \times 0.5°$–$2.5°$ 23 levels
Ocean initial conditions	Ocean analyses forced by ERA-40	Ocean analyses forced by ERA-40	Coupled run relaxed to observed SSTs
Reference	Wolff et al. (1997)	Madec et al. (1997)	Marsland et al. (2003)
Ensemble generation	Wind stress and SST perturbations	Wind stress and SST perturbations	Nine different atmospheric conditions from the coupled initialization run (lagged method)

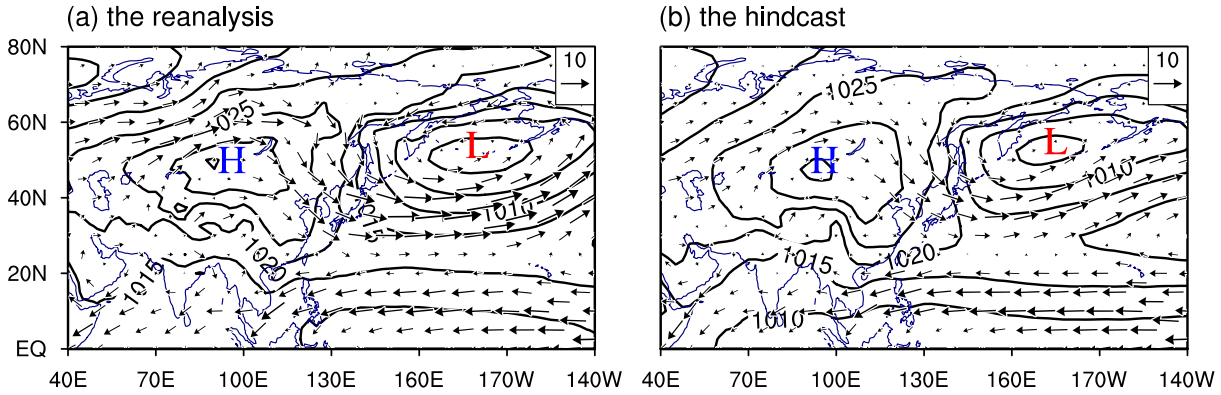

Fig. 1. Climatological-mean circulation over Eurasia and the North Pacific included SLP with contours (every 5 hPa) and UV850 with arrows (scaling given in the upper-right corner; units: m s^{-1}), for the period 1969–2001, in (a) the reanalysis and (b) the hindcast by the three-model ensemble. "H" and "L" denote centers of high and low pressure, respectively.

examined included sea level pressure (SLP), surface air temperature (SAT), air temperature at 850 hPa (T850), wind vector at 850 hPa (UV850), geopotential height at 500 hPa (HGT500), and zonal wind at 200 hPa (U200). The ERA-40 model was also used because NCEP-1 data over East Asia may contain systematic errors in the period prior to 1980 (Wu et al., 2005). (Note that the winter of 1969 refers to the 1969/1970 winter.)

First, the wintertime-mean circulation over Eurasia and North Pacific, including SLP and UV850 and produced by the three-model ensemble for the period 1969–2001, was compared with that derived from the reanalysis data (Fig. 1). The comparison reveals that two semipermanent surface pressure systems, the Siberian high and the Aleutian low, were well simulated over Eurasia and the North Pacific at mid- and-high latitudes, respectively. The reproduced central pressure of the Siberian high (1035 hPa) agreed closely with observation data, whereas the central pressure of Aleutian low (1005 hPa) had a positive bias of 5 hPa. In addition, the near-surface monsoonal flow was also well simulated; it extended from Siberia all the way down to the northern South China Sea, although in the three-model ensemble, the intensity tended to be slightly underestimated.

3. Hindcasts on the EAWM index

The spatial patterns of the first EOF mode of wintertime-mean T850 within the EAWM domain (20°–60°N, 90°–150°E) in the individual models and the three-model ensemble were compared with those derived from the reanalysis data (Fig. 2). In the comparison, the first mode derived from the reanalysis data accounted for 49.75% of the total variance, and the first mode derived from the hindcast data accounted for 39.36%–44.16% of the total variance. In addition, the leading mode derived from the reanalysis data was characterized by a cold center of −1.6°C located in central Siberia, with its amplitude decreasing southward. The leading modes derived from the simulations exhibited a similar but weaker feature. Note that the three-model ensemble mean result yielded a cold center of only −0.4°C.

Because the reproduced fluctuations of the leading mode were generally weaker, the pattern correlation coefficient (PCC) was employed as a measure of spatial consistency between the empirical orthagonal function (EOF) pattern from the models and the EOF pattern derived from the reanalysis data (Table 2). According to a Student's t-test, all values were statistically significant at a confidence level of 99%. The leading mode produced by the MME correlated with

Table 2. The PCC skills of the first EOF mode of winter-mean T850 within the EAWM domain. According to a Student's t-test, all values were statistically significant at a confidence level of 99%.

	ECMWF	Météo-France	MPI	MME
NCEP-1	0.858	0.477	0.545	0.839
ERA-40	0.850	0.478	0.459	0.794
Averaged	0.860	0.482	0.503	0.820

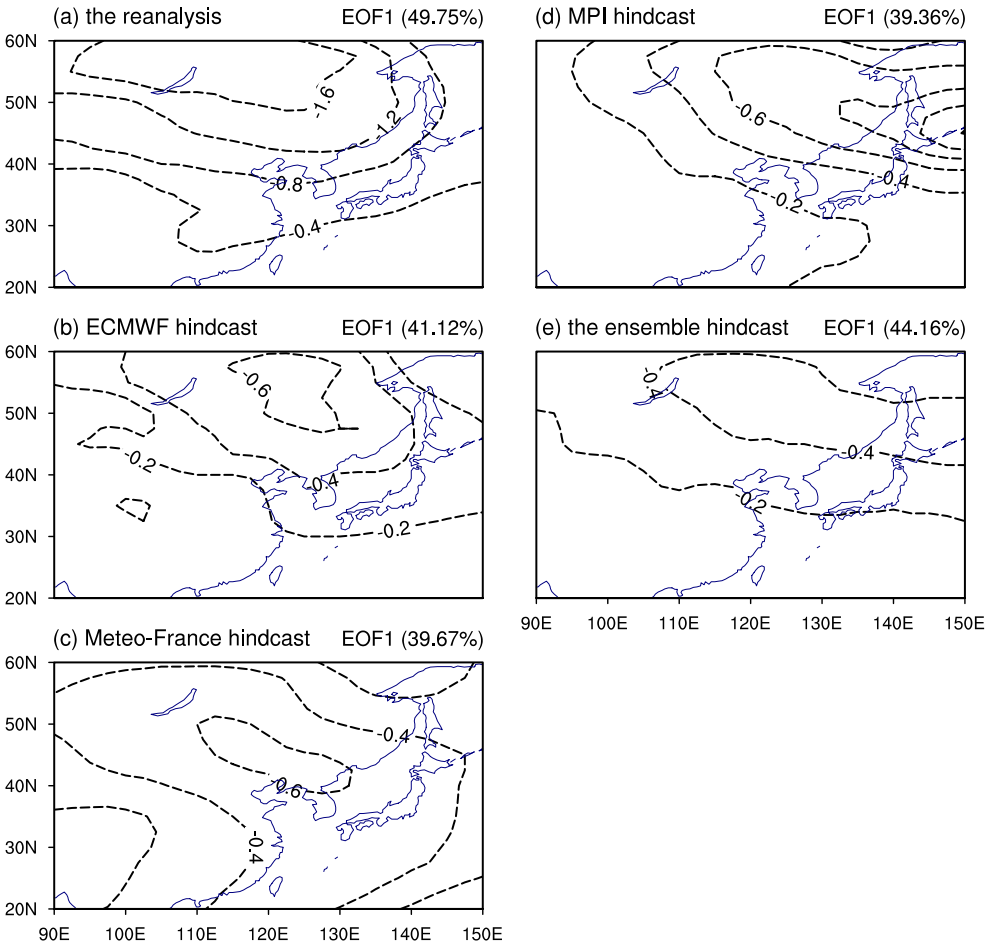

Fig. 2. Spatial pattern of the first EOF mode of wintertime-mean T850 within the EAWM domain in (a) the reanalysis with contours (every 0.4°C), (b) ECMWF hindcast, (c) Meteo-France hindcast, (d) MPI hindcast, and (e) the hindcast by the three-model ensemble, all with contours every 0.2°C. The numbers in parentheses denote the contribution to the total variances. Dashed lines indicate negative values.

the leading mode derived from the average of the two reanalysis up to 0.820, suggesting that the MME was able to replicate the spatial structure even though the intensity was underestimated.

The principal components (PCs) of the first EOF mode in the individual models and the three-model ensemble were plotted together with those derived from the reanalysis data (unnormalized; Fig. 3). The PCs produced by the models were broadly similar, and all agreed reasonably well with the PCs derived from the reanalysis data, but some PCs were radically different. The MPI model exhibited a relatively large bias between 1977 and 1985 and around 1992; TCCs are shown in Table 3. According to a Student's t-test, all values were statistically significant at a confidence level of 95%. Further, the MME yields a PC of 0.595 (Student's t-test showed a 99% confidence level), which was significantly higher than the results from individual

Table 3. The TCC skills of the PC of wintertime mean T850 within the EAWM domain. According to a Student's t-test, all values were statistically significant at a confidence level of 95%. Statistically significant values at 99% confidence level are shown in bold.

	ECMWF	Météo-France	MPI	MME
NCEP-1	0.419	**0.513**	0.401	**0.603**
ERA-40	0.413	**0.500**	0.386	**0.585**
Averaged	0.417	**0.508**	0.393	**0.595**

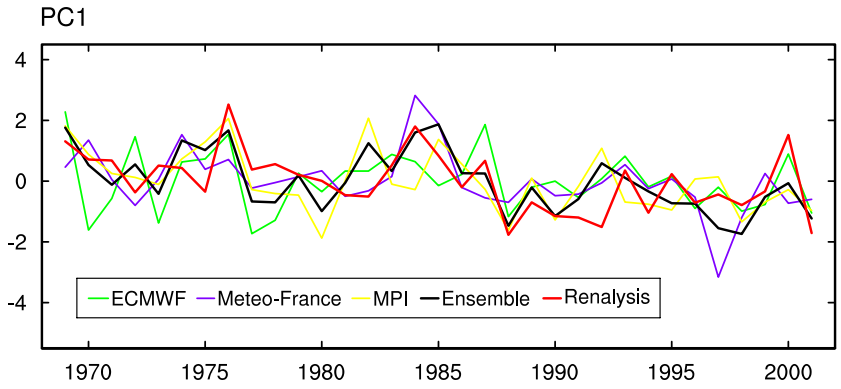

Fig. 3. Principal components of the first EOF mode derived from the reanalysis data and the hindcast by ECMWF, Meteo-France, MPI, and the three-model ensemble (unnormalized).

models (0.393–0.508). It is evident that the temporal behavior is well captured by the models, particularly by the three-model ensemble. Therefore, we propose an EAWM index that comprises the first EOF mode of the wintertime-mean T850 within the EAWM domain (20°–60°N, 90°–150°E). Our results show that the new EAWM index is affected by AO while it is ENSO independent, which is similar to results associated with the northern temperature mode (30°–60°N, 100°–140°E) presented by Wang and Chen (2010).

4. Hindcasts on the EAWM circulation interannual variability

In this section, we present the results of our evaluation of model performance in reproducing EAWM-related atmospheric circulation and temperature over Eurasia. The geographic distribution of TCCs in terms of HGT500, U850, SLP, U200, and SAT are plotted in Fig. 4. Importantly, dotted values were statistically significant at a confidence level of 95%, using a Student's t-test. Over the Indo-Pacific oceans, TCCs were observed to be generally high, similar to other models (Wang et al., 2009a). At 500 hPa, high TCCs were observed in a wave-train-like pattern over the Ural Mountains, East Asia, and the North Pacific (Fig. 4a). At 850 hPa, high TCCs were characterized by three clear pathways of the cold monsoonal flow (Fig. 4b): an eastward flow off the continent (known as the Eastern Pathway), a flow along the eastern flank of the Mongolian Plateau toward southern Japan (known as the Northwestern Pathway), and a third flow along the eastern flank of Tibetan Plateau toward the South China Sea (known as the Western Pathway).

Two well-detected SLP centers occurred in northern Eurasia and the North Pacific, respectively (Fig. 4c). In the upper troposphere, high accuracy was confined to the entrance region of the East Asian jet stream rather than the central region just over the south of Japan (Fig. 4d). Notably, the predictive ability of SAT was high over East Asia (Fig. 4e), which was consistent with the EOF analysis domain (20°–60°N, 90°–150°E) shown in the previous section. Overall, the areas with high TCCs were associated with the regimes of EAWM circulation. This agreement demonstrates the reasonable ability of the MME to predict the interannual variability of the EAWM and its major components.

Next we further explored the predictability of anomalous circulation and temperature for typical EAWM years. Because the EAWM underwent an interdecadal variation from the late 1980s (see Fig. 3), we first divided the data period into two subperiods: 1969–1985 and 1986–2001. For each subperiod, the typical EAWM years were identified as the absolute normalized values of the EAWM index larger than 1.0 standard deviation. According to this criterion, for the active EAWM period 1969 to 1985, three strong EAWM years (1969, 1976, 1984) and four weak EAWM years (1972, 1975, 1981, 1982) were identified. For the inactive EAWM period 1986 to 2001, three strong EAWM years (1987, 1993, 2000) and three weak EAWM years (1988, 1992, 2001) were identified. The groups were divided to verify the possible difference in the interannual variability between the active and inactive EAWM interdecadal backgrounds.

Figure 5 compares the anomalous circulation and temperature for the three strong EAWM years along with the climatology before the mid-1980s (Strong I), in terms of HGT500, UV850, SLP, U200, and SAT, between the reanalysis data and the hindcast ensemble. According to a Student's t-test, shaded values were statistically significant at a confidence level of 95%. At 500 hPa, a positive anomaly was detected

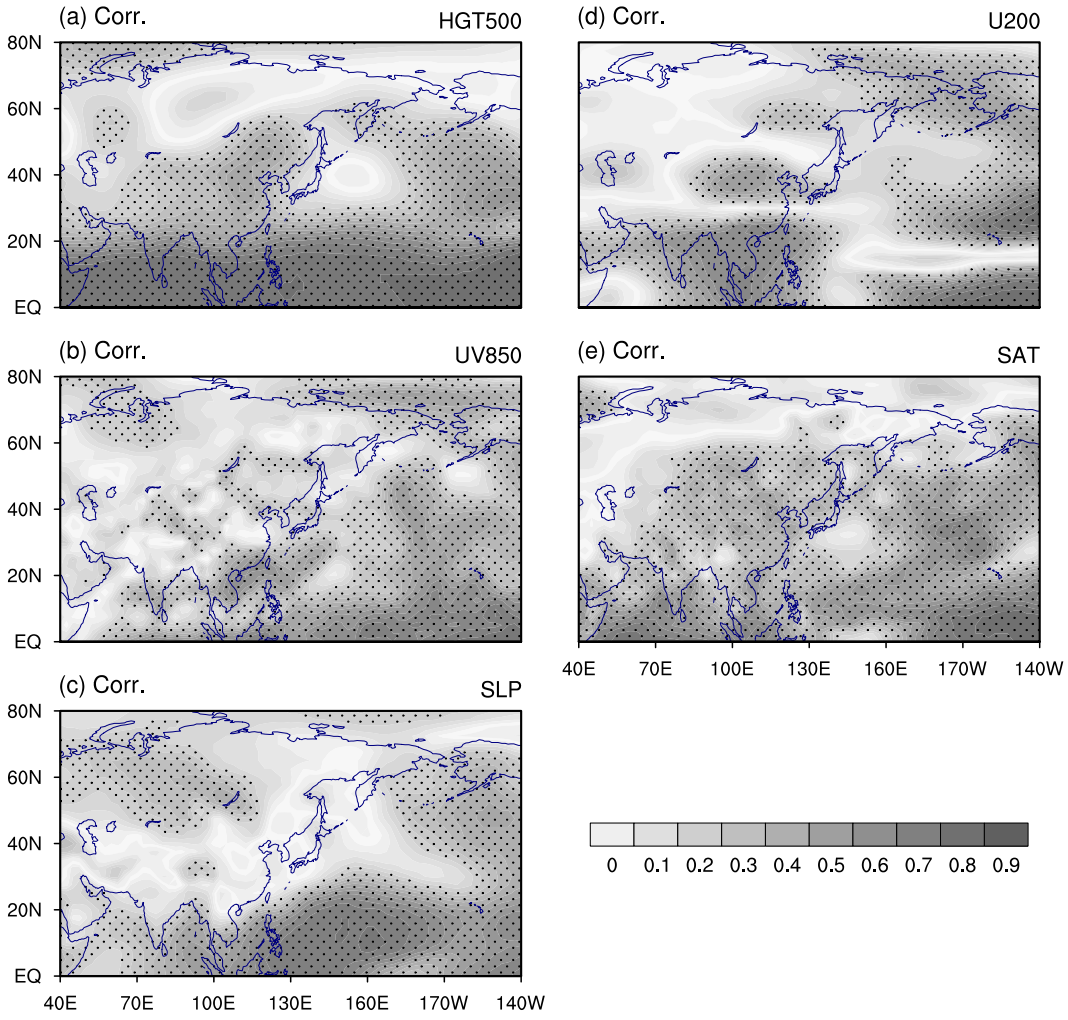

Fig. 4. The geographic distribution of TCCs in terms of (a) HGT500, (b) U850, (c) SLP, (d) U200, and (e) SAT. According to a Student's t-test, dotted values were statistically significant at a confidence level of 95%.

near the Kara Sea, with a negative anomaly centered over both Lake Baikal and the North Pacific, forming the extremely tight meridional gradient there (Fig. 5a). This structure closely resembles the structure of wintertime blocking over the Ural Mountains. At 850 hPa, associated low-level winds were enhanced in the polar region as well as at ~40°N over the East Asian–North Pacific sector (Fig. 5b). The SLP anomaly exhibited a dipole pattern with a positive polarity over northern Eurasia, which was controlled by the Siberia high. A weaker negative polarity can be seen in the North Pacific, where the Aleutian low is located (Fig. 5c). In the upper troposphere, the positive maximum can be seen along and downstream of the East Asian westerly jet (Fig. 5d). The prominent temperature feature is the large negative anomaly that occurred over northern Eurasia and extended down to central and southern China, with a center of −2°C north of 50°N (Fig. 5e).

Thus, the intensified Siberia high, Aleutian low, mid-to-upper-level high Ural blocking, and accelerated upper-troposphere East Asian westerly jet were coupled. Together, they may be viewed as an integrated, anomalously strong, EAWM circulation system. All of the anomaly patterns produced by the models agreed closely with those derived from reanalysis data, but the intensity tended to be somewhat underestimated. In terms of the circulation components, for HGT500 a positive bias of 7 gpm occurred over the Ural Mountains with a negative bias of −3 gpm over North Pacific (Fig. 5f). For SLP a positive bias of 7 hPa occurred over the Ural Mountains with a negative bias of −2 hPa over North Pacific (Fig. 5h). These factors may have artificially exaggerated the effect of Aleutian low, especially on associated low-level winds over the East Asian–North Pacific sector (Fig. 5g). In terms of

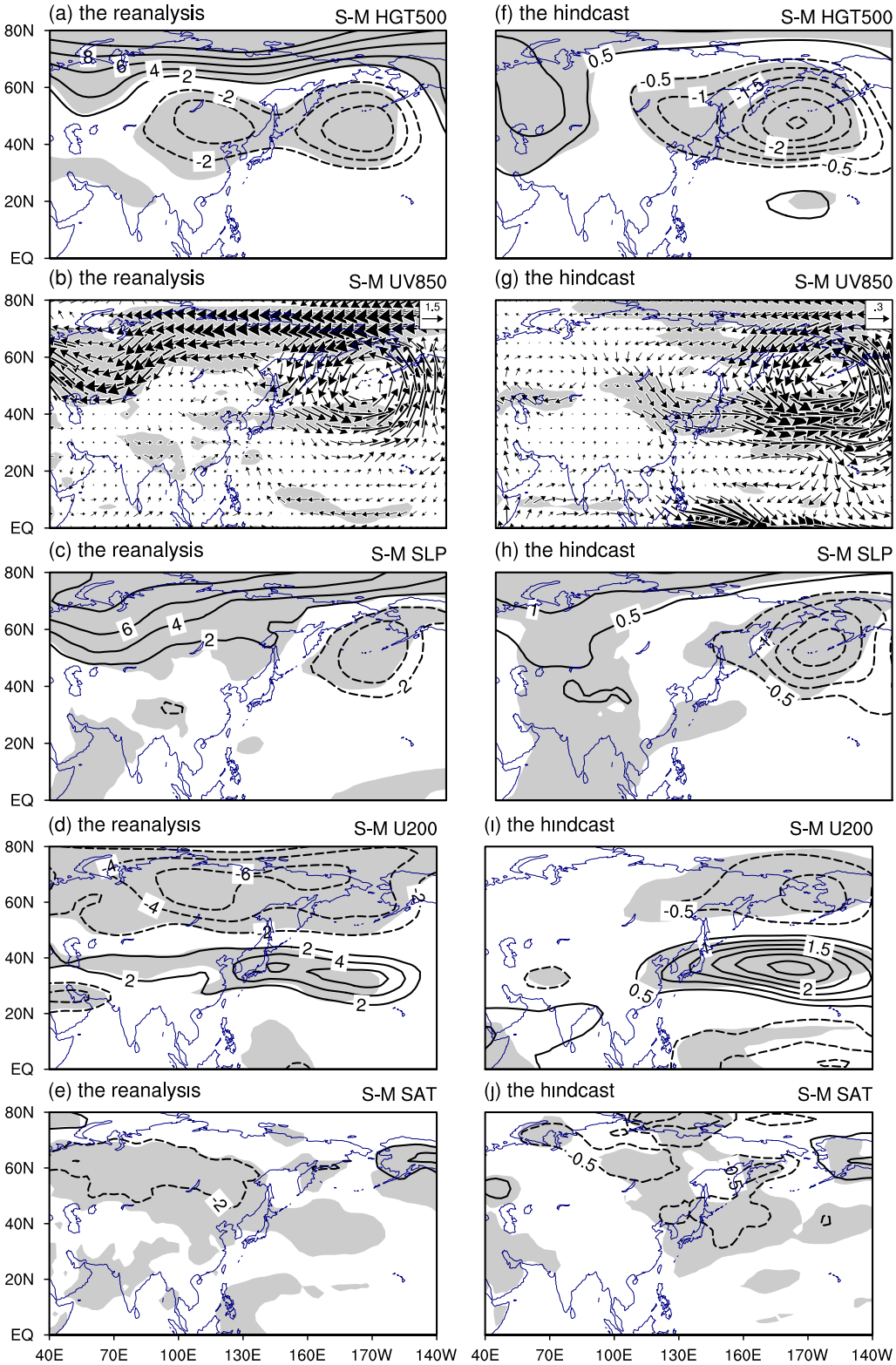

Fig. 5. Anomalous circulation and temperature for three strong EAWM years along with the climatology before the mid-1980s, in terms of HGT500 with contours every 2 gpm, UV850 with arrows (scaling given in the upper-right corner; units: m s^{-1}), SLP with contours every 2 hPa, U200 with contours every 2 m s^{-1}, and SAT with contours every 2°C, in (a–e) the reanalysis data and (f–j) the hindcast ensemble. According to a Student's *t*-test, shaded values were statistically significant at a confidence level of 95%.

the temperature, the MME intensity was only 25% of that produced using the reanalysis data. The PCCs of anomalies before and after the mid-1980s are presented in Table 4, as a measure of spatial consistency between the reproduced and the reanalyzed anomaly fields. According to a Student's t-test, all values were statistically significant at a confidence level of 99%. The prediction of the anomalous circulation yielded anomaly PCCs of 0.499–0.834. The prediction of the temperature was physically reliable, yielding an anomaly PCC of 0.351.

Figure 6 shows three strong EAWM years along with the climatology after the mid-1980s. The anomalous circulation and temperature show an obvious weakening trend compared with those before the mid-1980s (Strong II). At 500 hPa, a weaker positive anomaly can be seen near the Kara Sea, with a negative anomaly centered over Lake Baikal and the Northwest Pacific (Fig. 6a). The SLP anomalies show a weaker dipole (Fig. 6c), together with the westerlies at both the upper and lower troposphere at ∼40°N over the East Asian–North Pacific sector (Figs. 6b and d). The temperature shows a negative center of −4°C north of 50°N (Fig. 6e).

The anomalies after the mid-1980s produced by the models show patterns similar to that derived from the reanalysis data. In terms of the circulation components, the difference for HGT500 is associated with the negative anomaly extending from North Pacific westward to Europe, which misses the wintertime blocking over the Ural Mountains (Fig. 6f). In addition, the zero contour line in SLP can be seen farther north of 60°N over Eurasia (Fig. 6h). The PCCs of the anomalous circulation were 0.414–0.802, and the prediction accuracy of the temperature was 0.288 (see Table 4).

Figure 7 compares the anomalous circulation and temperature for four weak EAWM years along with the climatology before the mid-1980s (Weak I), in terms of HGT500, UV850, SLP, U200, and SAT, derived from the reanalysis data and from the hindcast ensemble. Notably, the anomaly patterns resemble those for the three strong EAWM years after the mid-1980s, with a negative signal. At 500 hPa, a negative anomaly can be seen near the Kara Sea, with a positive anomaly extending from the North Pacific westward to Lake Baikal, which reflects a reduced meridional gradient (Fig. 7a). The SLP anomaly exhibits a dipole pattern with a negative polarity over northern Eurasia and a positive polarity in the North Pacific (Fig. 7c). The westerlies are weakened at both the upper and lower troposphere at ∼40°N over the East Asian–North Pacific sector (Figs. 7b, d). In addition, the temperature exhibits a positive center of 2°C north of 50°N (Fig. 7e).

Here, the models captured the major circulation components that decreased and the extreme warm temperatures, but they failed to capture the weaker signals over northern Eurasia generally. This may be a primary reason that the anomaly PCCs of the circulation fields merely ranged from 0.110 to 0.222 (see Table 4). The prediction accuracy of the temperature even dropped below zero (−0.064).

Figure 8 shows the three weak EAWM years along with the climatology after the mid-1980s. The anomaly patterns are opposite for the three strong EAWM years before the mid-1980s. Strong EAWM circulation patterns are consistent with an active background, whereas weak EAWM circulation are consistent with an inactive background, meaning that strong EAWM periods tend to have stronger EAWM years and weak EAWM periods tend to have weaker years.

The models captured the circulation components that decreased and the extreme warm temperatures after the mid-1980s. The anomaly PCCs of the circulation fields were up to 0.481–0.787, and the prediction accuracy regarding temperature was 0.135 (see Table 4). Overall, our results show that the strong EAWM was much stronger for the previous observation period, and that the weak EAWM was much weaker for the later observation period. This important feature representing the interdecadal variation of EAWM was reasonably simulated by the models. In addition, in terms of Strong I, Strong II, and Weak II, the anomaly PCCs of the circulation fields range from 0.414 to 0.834, and the prediction accuracy of the temperature ranged from 0.135 to 0.351. In terms of Weak I, the anomaly PCCs of the circulation fields merely ranged from 0.110 to 0.222, and the prediction accuracy of the temperature even dropped below zero (−0.064) because the models missed the weaker signals over northern Eurasia in general.

5. Discussion and summary

This study focused on the validation of the DEMETER hindcast for EAWM interannual variability. A new EAWM index was defined to describe the general features of the EAWM. Results show that the EAWM index can be well simulated by the models, particularly by the three-model ensemble.

In addition, areas with high TCCs were shown to be under the influence of the EAWM circulation system. This agreement demonstrates the reasonable ability of the models to predict the interannual variability of the EAWM and its major components.

We further compared the anomalous circulation and temperatures for typical EAWM years, along with the climatology before and after the mid-1980s. The

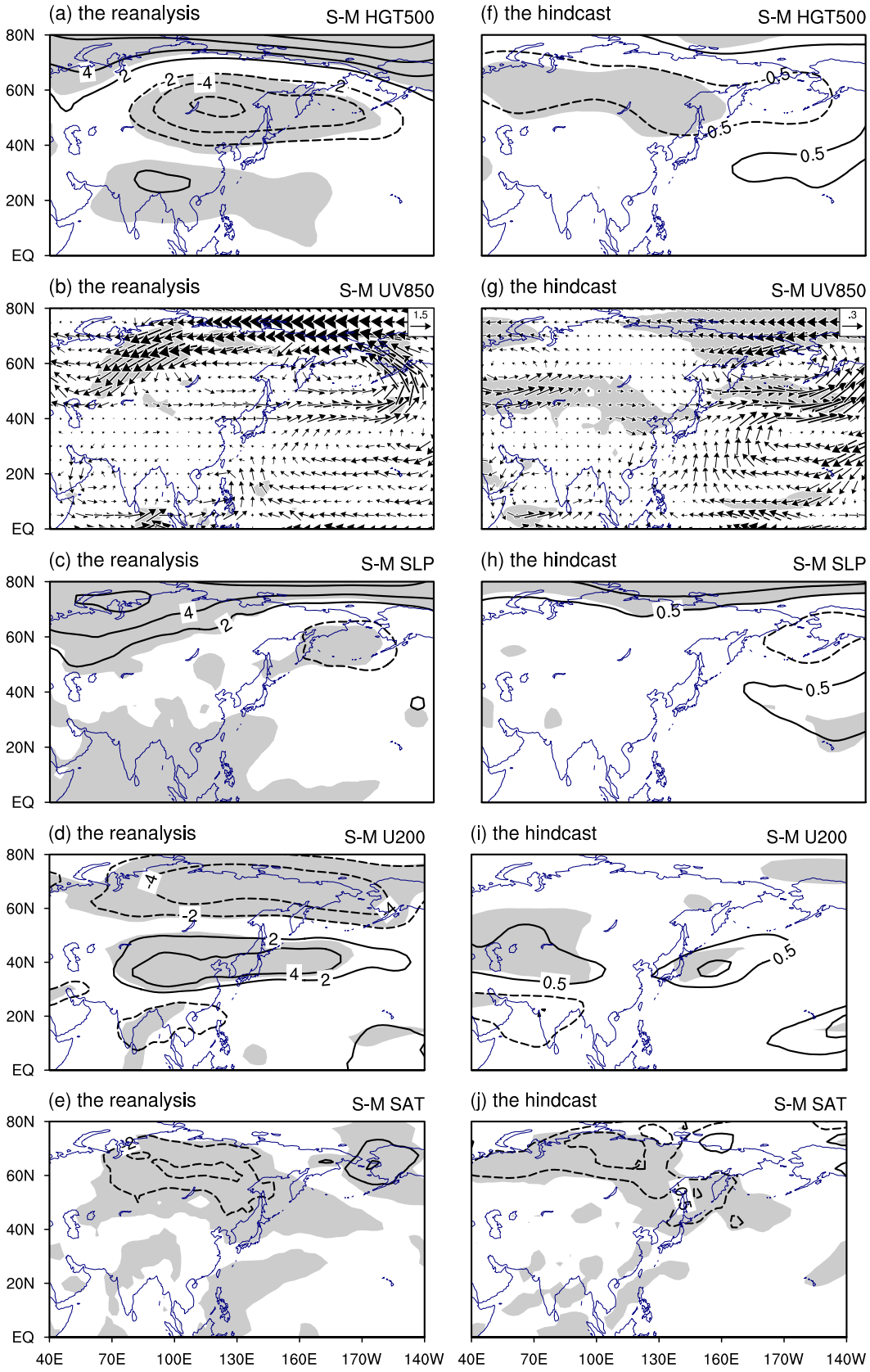

Fig. 6. Same as Fig. 5 but for three strong EAWM years along with the climatology after the mid-1980s.

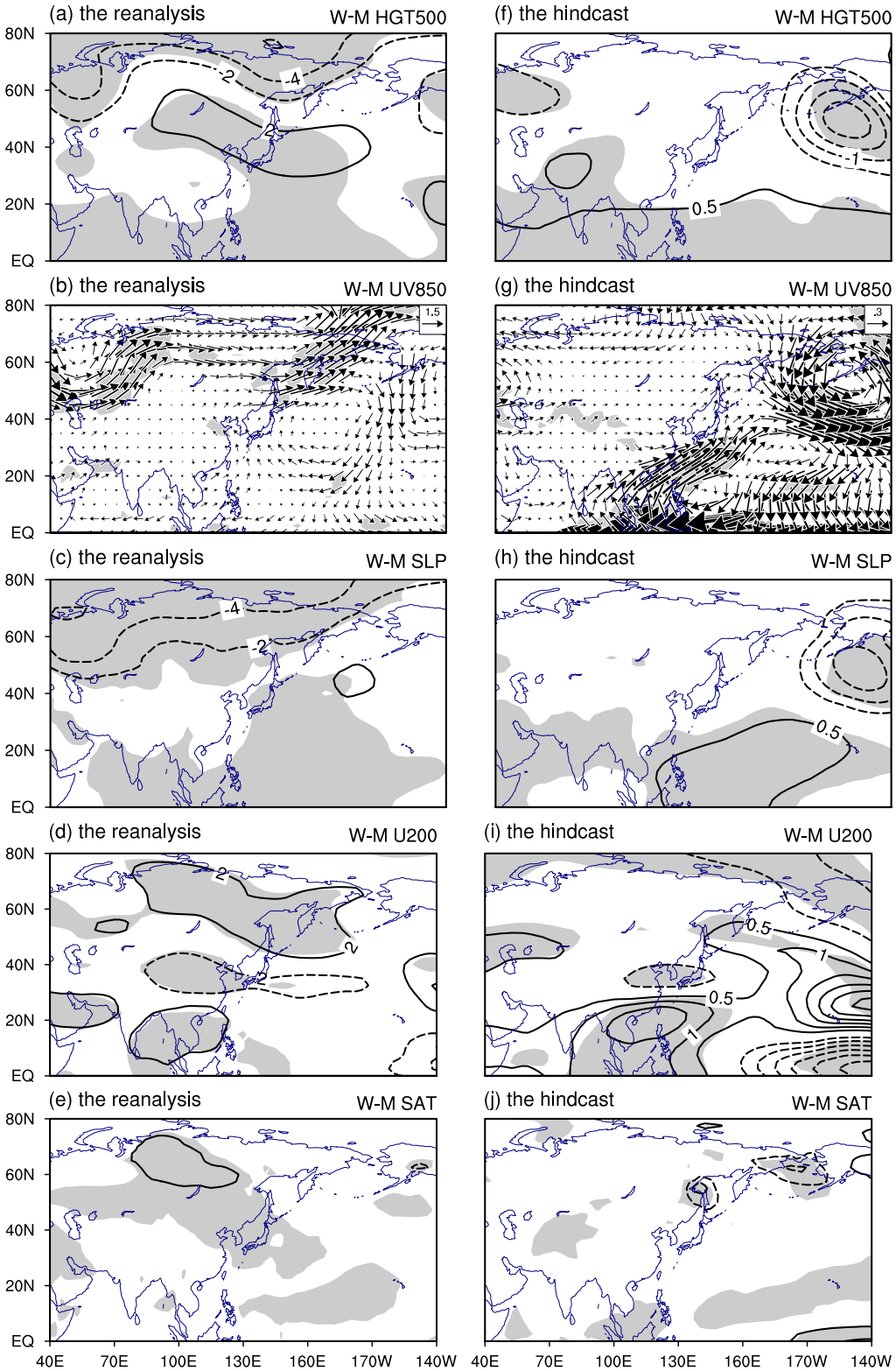

Fig. 7. Anomalous circulation and temperature for four weak EAWM years along with the climatology before the mid-1980s, in terms of HGT500 with contours every 2 gpm, UV850 with arrows (scaling given in the upper-right corner; unit: m s^{-1}), SLP with contours every 2 hPa, U200 with contours every 2 m s^{-1}, and SAT with contours (every 2°C), in (a–e) the reanalysis data and (f–j) the hindcast ensemble. According to a Student's *t*-test, shaded values were statistically significant at a confidence level of 95%.

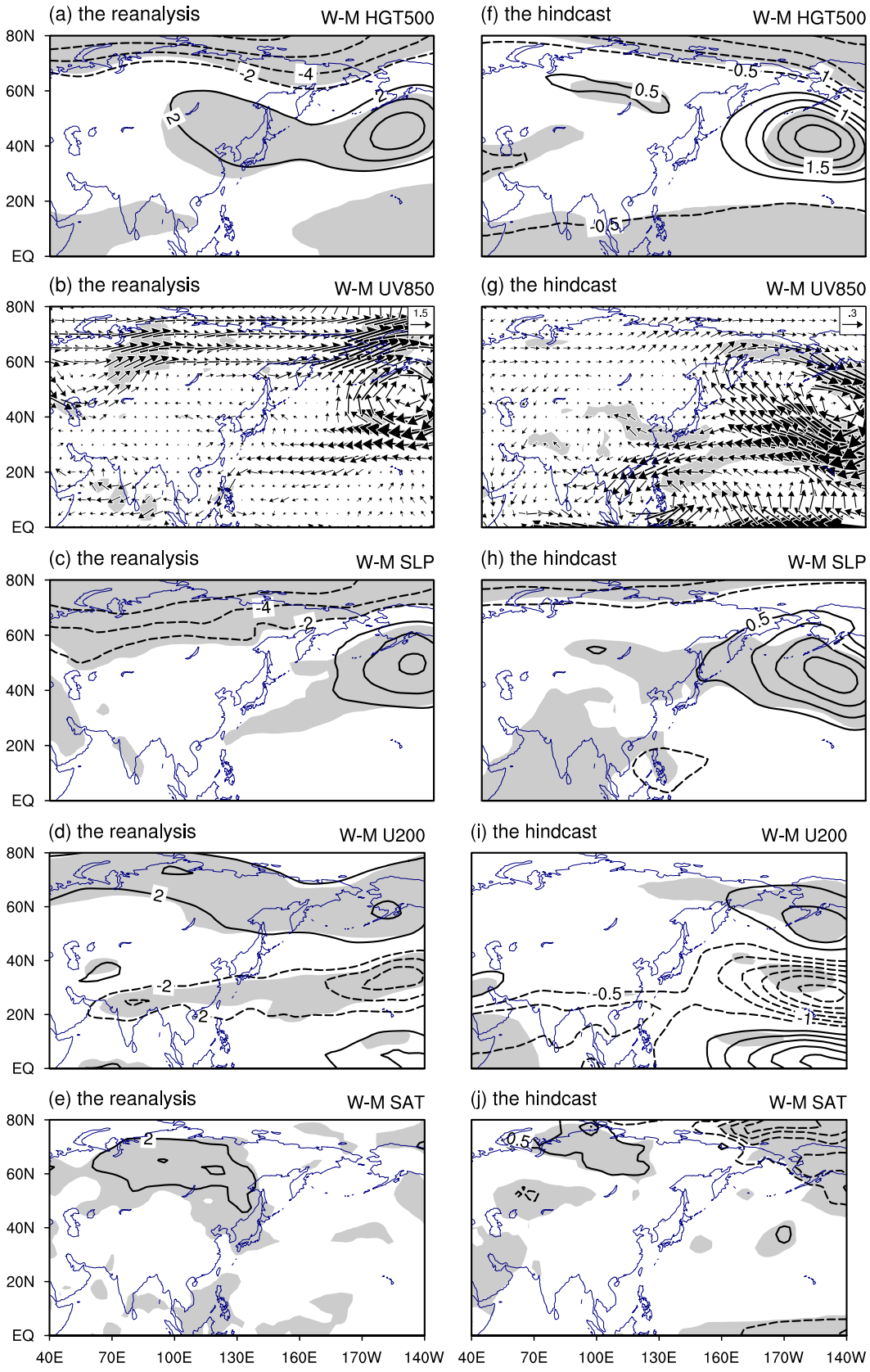

Fig. 8. Same as Fig. 5 but for three weak EAWM years along with the climatology after the mid-1980s.

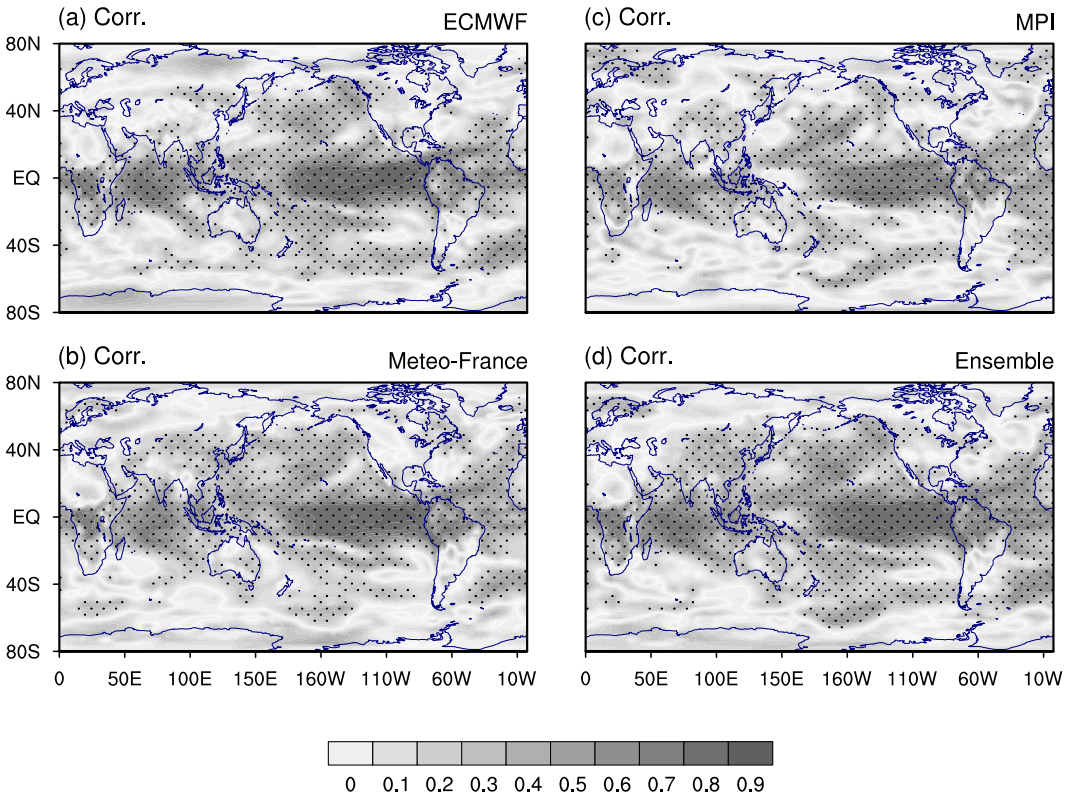

Fig. 9. The geographic distribution of TCCs of SAT in (a) the ECMWF hindcast, (b) the Meteo-France hindcast, (c) the MPI hindcast, and (d) the hindcast by the three-model ensemble. According to a Student's t-test, dotted values were statistically significant at a confidence level of 95%.

strong EAWM was much stronger during the earlier observation period, and the weak EAWM was much weaker for the later observation period. This important feature representing the interdecadal variation of EAWM can be simulated by the prediction system of the models, except for a general underestimation of the related anomalies.

Thus our results offer a promising conclusion: the models have some ability to predict both the interannual and interdecadal variability of EAWM. The major bias of the models is the underestimation of the related anomalies.

The physical basis of EAWM predictability is closely associated with that of SST (particularly the ENSO) predictability, which exerts significant influence on the direct monsoonal circulation over East Asia. Because the 1-month lead-time prediction strategy was applied, relatively accurate prediction of the SST was obtained. The geographic distribution of TCCs of SAT in the individual models and the three-model ensemble are plotted in Fig. 9. According to a Student's t-test, dotted values were statistically significant at a confidence level of 95%. The high accuracy of SST prediction is well demonstrated by the results of SAT. We see that TCCs are significantly high at most mid- and low-latitudes, with the largest TCCs around the globe occurring in the tropical oceans. The predictive accuracy for Asia is also quite good, better than in other regions at the same latitudes. However, the low predictability of the AO as revealed by Qian et al. (2011) can lead to uncertainty in predicting the EAWM. This is due to the modulation effect of the

Table 4. The anomaly PCC skills of the circulation fields and the temperature before and after the mid-1980s (I and II). According to a Student's t-test, all values were statistically significant at a confidence level of 99%.

	HGT500	UV850	SLP	U200	SAT
Strong I	0.708	0.499/0.476	0.834	0.548	0.351
Strong II	0.646	0.538/0.392	0.802	0.414	0.288
Weak I	0.184	0.110/0.019	0.222	0.205	−0.064
Weak II	0.732	0.481/0.209	0.787	0.635	0.135

AO on the EAWM, as indicated by Gong et al. (2001), Wang and Sun (2009), and others.

Acknowledgements. This work was supported by the Major State Basic Research Development Program of China (973 Program, Grant No. 2009CB421406), the National Natural Science Foundation of China (Grant Nos. 41130103 and 40821092), the Special Fund for Public Welfare Industry (Meteorology, Grant No. GYHY200906018), and the Norwegian Research Council "East Asia DecCen" Project.

REFERENCES

Chen, W., S. Yang, and R. H. Huang, 2005: Relationship between stationary planetary wave activity and the East Asian winter monsoon. *J. Geophys. Res.*, **110**, D14110.

Cui, X. P., and Z. B. Sun, 1999: East Asian winter monsoon index and its variation analysis. *Journal of Nanjing Institute of Meteorology*, **22**, 321–325. (in Chinese)

Déqué, M., 2001: Seasonal predictability of tropical rainfall: Probabilistic formulation and validation. *Tellus*, **53A**, 500–512.

Fan, K., 2009: Predicting winter surface air temperature in Northeast China. *Atmos. Oceanic Sci. Lett.*, **2**, 14-17.

Gong, D. Y., S. W. Wang, and J. H. Zhu, 2001: East Asian winter monsoon and Arctic Oscillation. *Geophys. Res. Lett.*, **28**, 2073–2076.

Gregory, D., J. J. Morcrette, C. Jakob, A. C. M. Beljaars, and T. Stockdale, 2000: Revision of convection, radiation and cloud schemes in the ECMWF Integrated Forecasting System. *Quart. J. Roy. Meteor. Soc.*, **126**, 1685–1710.

Guo, Q. Y., 1994: Relationship between the variations of East Asian winter monsoon and temperature anomalies in China. *Quarterly Journal of Applied Meteorological*, **5**, 218–225. (in Chinese)

Han, Z., S. L. Li, and M. Mu, 2011: The role of warm North Atlantic SST in the formation of positive height anomalies over the Ural Mountains during January 2008. *Adv. Atmos. Sci.*, **28**, 246–256, doi: 10.1007/s00376-010-0069-1.

Jhun, J. G., and E. J. Lee, 2004: A new East Asian winter monsoon index and associated characteristics of the winter monsoon. *J. Climate*, **17**, 711–726.

Ji, L. R., S. Q. Sun, K. Arpe, and L. Bengtsson, 1997: Model study on the interannual variability of Asian winter monsoon and its influence. *Adv. Atmos. Sci.*, **14**, 1–22.

Kalnay, E., and Coauthors, 1996: The NCEP/NCAR 40-Year Reanalysis Project. *Bull. Amer. Meteor. Soc.*, **77**, 437-471.

Lau, N. C., and M. J. Nath, 2000: Impact of ENSO on the variability of the Asian-Australian monsoons as simulated in GCM experiments. *J. Climate*, **13**, 4287–4309.

Madec, G., P. Delecluse, M. Imbard, and C. Levy, 1997: OPA release 8, ocean general circulation model reference manual. LODYC Internal Rep., Paris, France, 200pp. [Available from LODYC/IPSL, 4 Place Jussieu 75252 Paris Cedex 05, France.]

Marsland, S. J., H. Haak, J. H. Jungclaus, M. Latif, and F. Röske, 2003: The Max-Planck-Institute global ocean/sea ice model with orthogonal curvilinear coordinates. *Ocean Modelling*, **5**, 91–127.

Palmer, T. N., and Coauthors, 2004: Development of a European multimodel ensemble system for seasonal-to-interannual prediction (DEMETER). *Bull. Amer. Meteor. Soc.*, **85**, 853–872.

Qian, Z. L., H. J. Wang, and J. Q. Sun, 2011: The hindcast of winter and spring Arctic and Antarctic Oscillation with the coupled climate models. *Acta Meteorologica Sinica*, **25**, 340–354.

Roeckner, E., 1996: The atmospheric general circulation model ECHAM-4: Model description and simulation of present-day climate. Max-Planck-Institut für Meteorologie Tech. Rep. 218, Hamburg, Germany, 90pp. [Available from Max-Planck Institut für Meteorologie, Bundesstr. 55, D-20146 Hamburg, Germany.]

Shi, N., and Y. S. Yang, 1998: Main characteristics of East Asian summer/winter monsoon index for 1873–1996. *Journal of Nanjing Institute of Meteorology*, **21**, 208–214. (in Chinese)

Sun, J. Q., H. J. Wang, W. Yuan, and H. P. Chen, 2010: Spatial-temporal features of intense snowfall events in China and their possible change. *J. Geophys. Res.*, **115**, D16110.

Takaya, K., and H. Nakamura, 2005a: Mechanisms of intraseasonal amplification of the cold Siberian high. *J. Atmos. Sci.*, **62**, 4423-4440.

Takaya, K., and H. Nakamura, 2005b: Geographical dependence of upper-level blocking formation associated with intraseasonal amplification of the Siberian high. *J. Atmos. Sci.*, **62**, 4441-4449.

Uppala, S. M., and Coauthors, 2005: The ERA-40 Re-Analysis. *Quart. J. Roy. Meteor. Soc.*, **131**, 2961–3012.

Wang, B., R. G. Wu, and X. H. Fu, 2000: Pacific-East Asian teleconnection: How does ENSO affect East Asian climate? *J. Climate*, **13**, 1517–1536.

Wang, B., and Coauthors, 2009a: Advance and prospectus of seasonal prediction: Assessment of the APCC/CliPAS 14-model ensemble retrospective seasonal prediction (1980–2004). *Climate Dyn.*, **33**, 93–117.

Wang, B., Z. W. Wu, C. P. Chang, J. Liu, J. P. Li, and T. J. Zhou, 2010: Another look at interannual-to-interdecadal variations of the East Asian winter monsoon: The northern and southern temperature modes. *J. Climate*, **23**, 1495–1512.

Wang, H. J., 2001: The weakening of the Asian monsoon circulation after the end of 1970's. *Adv. Atmos. Sci.*, **18**, 376–386.

Wang, H. J., and D. B. Jiang, 2004: A new East Asian

winter monsoon intensity index and atmospheric circulation comparison between strong and weak composite. *Quaternary Sciences*, **24**, 19–27. (in Chinese)

Wang, H. J., and J. Q. Sun, 2009: Variability of Northeast China river break-up date. *Adv. Atmos. Sci.*, **26**, 701–706, doi: 10.1007/s00376-009-9035-1.

Wang, H. J., E. T. Yu, and S. Yang, 2011: An exceptionally heavy snowfall in Northeast China: Large-scale circulation anomalies and hindcast of the NCAR WRF model. *Meteor. Atmos. Phys.*, **113**, 11–25.

Wang, L., and W. Chen, 2010: How well do existing indices measure the strength of the East Asian winter monsoon? *Adv. Atmos. Sci.*, **27**, 855–870, doi: 10.1007/s00376-009-9094-3.

Wang, L., W. Chen, and R. H. Huang, 2008: Interdecadal modulation of PDO on the impact of ENSO on the east Asian winter monsoon. *Geophys. Res. Lett.*, **35**, L20702.

Wang, L., W. Chen, W. Zhou, and R. H. Huang, 2009b: Interannual variations of East Asian trough axis at 500 hPa and its association with the East Asian winter monsoon pathway. *J. Climate*, **22**, 600–614.

Wang, L., R. H. Huang, L. Gu, W. Chen, and L. H. Kang, 2009c: Interdecadal variations of the East Asian winter monsoon and their association with quasi-stationary planetary wave activity. *J. Climate*, **22**, 4860–4872.

Webster, P. J., and S. Yang, 1992: Monsoon and ENSO: Selectively interactive systems. *Quart. J. Roy. Meteor. Soc.*, **118**, 877–926.

Wolff, J. E., E. Maier-Reimer, and S. Legutke, 1997: The Hamburg Ocean primitive equation model. Deutsches Klimarechenzentrum Tech. Rep. 13, Hamburg, Germany, 13pp. [Available from Model and Data Group c/o Max-Planck Institut für Meteorologie, Bundesstr. 55, D-20146 Hamburg, Germany.]

Wu, R., J. L. Kinter III, and B. P. Kirtman, 2005: Discrepancy of interdecadal changes in the Asian region between the NCEP-NCAR reanalysis and observations. *J. Climate*, **18**, 3048–3067.

Yan, H. M., W. Zhou, H. Yang, and Y. Cai, 2009: Definition of a East Asian winter monsoon index and its variation characteristics. *Transactions of Atmospheric Sciences*, **32**, 367–376. (in Chinese)

Zhang, C. J., and H. Q. Zhang, 2010: Potential impacts of East Asian winter monsoon on climate variability and predictability in the Australian summer monsoon region. *Theor. Appl. Climatol.*, **101**, 161–177.

Zhang, R., A. Sumi, and M. Kimoto, 1996: Impact of El Niño on the East Asian monsoon: A diagnostic study of the '86/87 and '91/92 events. *J. Meteor. Soc. Japan*, **74**, 49–62.

Zhang, Y., K. R. Sperber, and J. S. Boyle, 1997: Climatology and interannual variation of the East Asian winter monsoon: Results from the 1979–95 NCEP/NCAR reanalysis. *Mon. Wea. Rev.*, **125**, 2605–2619.

Zhou, W., J. C. L. Chan, W. Chen, J. Ling, J. G. Pinto, and Y. P. Shao, 2009: Synoptic-scale controls of persistent low temperature and icy weather over southern China in January 2008. *Mon. Wea. Rev.*, **137**, 3978–3991.

Zhu, C. W., W. S. Lee, H. W. Kang, and C. K. Park, 2005: A proper monsoon index for seasonal and interannual variations of the East Asian monsoon. *Geophys. Res. Lett.*, **32**, L02811.